Characterizing the structure of aerobic granular sludge using ultra-high field magnetic resonance

Kirkland, Catherine M. ; Seymour, Joseph D. ; Krug, Julia R.; Velders, Aldrik H.; Vergeldt, Frank J.; Van As, Henk; van den Berg, Lenno; de Kreuk, Merle K.; Codd, Sarah L.

DOI
10.2166/wst.2020.341

Publication date
2020

Document Version
Final published version

Published in
Water science and technology : a journal of the International Association on Water Pollution Research

Citation (APA)
Kirkland, C. M., Seymour, J. D., Krug, J. R., Velders, A. H., Vergeldt, F. J., Van As, H., van den Berg, L., de Kreuk, M. K., & Codd, S. L. (2020). Characterizing the structure of aerobic granular sludge using ultra-high field magnetic resonance. *Water science and technology : a journal of the International Association on Water Pollution Research*, *82*(4), 627-639. https://doi.org/10.2166/wst.2020.341

Characterizing the structure of aerobic granular sludge using ultra-high field magnetic resonance

Catherine M. Kirkland, Julia R. Krug, Frank J. Vergeldt, Lenno van den Berg, Aldrik H. Velders, Joseph D. Seymour, Sarah L. Codd, Henk Van As and Merle K. de Kreuk

ABSTRACT

Despite aerobic granular sludge wastewater treatment plants operating around the world, our understanding of internal granule structure and its relation to treatment efficiency remains limited. This can be attributed in part to the drawbacks of time-consuming, labor-intensive, and invasive microscopy protocols which effectively restrict samples sizes and may introduce artefacts. Time-domain nuclear magnetic resonance (NMR) allows non-invasive measurements which describe internal structural features of opaque, complex materials like biofilms. NMR was used to image aerobic granules collected from five full-scale wastewater treatment plants in the Netherlands and United States, as well as laboratory granules and control beads. T_1 and T_2 relaxation-weighted images reveal heterogeneous structures that include high- and low-density biofilm regions, water-like voids, and solid-like inclusions. Channels larger than approximately 50 μm and connected to the bulk fluid were not visible. Both cluster and ring-like structures were observed with each granule source having a characteristic structural type. These structures, and their NMR relaxation behavior, were stable over several months of storage. These observations reveal the complex structures within aerobic granules from a range of sources and highlight the need for non-invasive characterization methods like NMR to be applied in the ongoing effort to correlate structure and function.

Key words | aerobic granular sludge, biofilm, EPS, MRI, nuclear magnetic resonance, wastewater

HIGHLIGHTS

- Ultra-high field NMR imaging shows complex and heterogeneous structures in intact aerobic granules treating municipal wastewater.
- The structures were comprised of high- and low-density biofilm regions, water-like voids, and solid-like inclusions.
- Internal structural characteristics varied by granule source and were stable over at least 2 months of storage.
- NMR is sensitive to different physico-chemical parameters than traditional microscopy and can provide a new research perspective.
- NMR allows for non-invasive screening of larger sample sizes to explore the structure–function relationship.

Catherine M. Kirkland (corresponding author)
Department of Civil Engineering,
Montana State University,
205 Cobleigh, Bozeman, Montana, 59717,
USA
E-mail: *catherine.kirkland@montana.edu*

Catherine M. Kirkland
Joseph D. Seymour
Center for Biofilm Engineering,
Montana State University,
366 Barnard, Bozeman, Montana, 59717,
USA

Julia R. Krug
Aldrik H. Velders
Laboratory of BioNanoTechnology,
Wageningen University and Research,
Axis building, Bornse Weilanden 9, 6708 WG,
Wageningen,
The Netherlands

Julia R. Krug
Frank J. Vergeldt
Henk Van As
Laboratory of Biophysics and MAGNEtic Resonance Research FacilitY (MAGNEFY),
Wageningen University and Research,
Helix building, Stippeneng 4, 6708 WG,
Wageningen,
The Netherlands

Lenno van den Berg
Merle K. de Kreuk
Department of Water Management,
Delft University of Technology,
Stevinweg 1, 2628 CN, Delft,
The Netherlands

Joseph D. Seymour
Department of Chemical and Biological Engineering,
Montana State University,
306 Cobleigh, Bozeman, Montana, 59717,
USA

Sarah L. Codd
Department of Mechanical and Industrial Engineering,
Montana State University,
220 Roberts, Bozeman, Montana, 59717,
USA

doi: 10.2166/wst.2020.341

INTRODUCTION

Compared to conventional activated sludge systems, aerobic granular sludge (AGS) offers numerous benefits for wastewater treatment including compact design, lower energy costs, and excellent biomass retention (de Bruin *et al.* 2004). In the last two decades, research into the formation, structure, and metabolism of granular sludge has flourished (Tay *et al.* 2001; Beun *et al.* 2002; de Kreuk & van Loosdrecht 2006; Wilen *et al.* 2018) and numerical models have been developed to simulate substrate removal, the distribution of microbial populations, and biochemical processes within the biofilm granule (Xavier *et al.* 2007; Kagawa *et al.* 2015). Today, full-scale reactors are in operation around the world (Pronk *et al.* 2017).

Numerous studies have reported heterogeneous internal structures in aerobic granules from various sources (McSwain *et al.* 2005; Chen *et al.* 2007; Lemaire *et al.* 2008; Liu *et al.* 2010; Gonzalez-Gil & Holliger 2014; Weissbrodt *et al.* 2015). Typical methods of analysis include use of fixatives, fluorescent *in situ* hybridization (FISH) probes, or staining with fluorophores followed by cryo-sectioning and imaging with confocal microscopy to identify the spatial arrangement of cells and biopolymers like proteins and polysaccharides within the granules. These types of studies have revealed microbial communities occupying niche environments within the granule architecture as well as the presence of voids and channels in the granule interior. This study, for the first time, applied ultra-high field nuclear magnetic resonance (NMR) to explore the structural heterogeneity of aerobic granular sludge from full-scale municipal wastewater treatment reactors, as well as from laboratory-scale reactors.

Time-domain NMR can provide spatially resolved data on the structure and water diffusivity present in intact granules under various hydrodynamic conditions (Van As & Lens 2001; Codd *et al.* 2006). Early NMR experiments on anaerobic granules provided evidence of a cluster structure (Gonzalez-Gil *et al.* 2001), while NMR imaging of methanogenic granules showed that the matrix of extracellular polymeric substances (EPS) is organized in concentric layers and the granules appear to have hollow centers (Lens *et al.* 2003). While the achievable spatial resolution is less than that typically obtained with optical methods, magnetic resonance is non-destructive and non-invasive. It can be used to image opaque and heterogeneous samples by exploiting the contrasts between the NMR signal intensity and decay rates associated with various granule components. In this research paper, the additional use of state-of-the-art ultra-high magnetic field strength (22.3 Tesla (T) or 950 MHz where $\mathrm{MHz} = \mathrm{T}\gamma$ and γ is 2.675×10^8 rad/(s*T) for protons) allows for enhanced contrast between various biochemical macromolecules and fast, high-resolution imaging. Moreover, the sensitivity of NMR to molecular motion provides an opportunity to observe the inherent transport characteristics of a system *in situ* in relation to structure (Van As & Lens 2001). These capabilities represent significant advantages compared to conventional methods like microscopy and micro-electrode studies which are necessarily invasive or destructive. Thus, because NMR is sensitive to a different array of physical and chemical parameters than traditional microscopy methods and can be used to screen larger sample sizes non-invasively, NMR imaging has the potential to highlight structural features that might otherwise not be visible, providing complementary data to inspire new research questions.

The primary research questions addressed here are related to the internal granule structure. To what extent does the internal structure of aerobic granules used in practice for wastewater treatment conform to a layered (Lens *et al.* 2003) or cluster (Gonzalez-Gil *et al.* 2001) conceptual model? How consistent are the observed structures between samples from the same treatment plant, from different treatment plants, over time as the granules age, and between laboratory granules and those treating municipal wastewater? NMR imaging experiments and T_1–T_2 relaxation correlation experiments (see Methods section) give insight to these structural questions. Complementary NMR studies have begun to explore how diffusive transport varies within a granule with respect to structural features.

METHODS

Sample collection and preparation

Samples of aerobic granular sludge were collected during the aeration phase of the treatment cycle from the following sequencing batch reactors (SBRs): full-scale Garmerwolde (The Netherlands), full-scale Vroomshoop (The Netherlands), prototype Utrecht (PNU) (The Netherlands), and demonstration-scale Rockford (IL, USA). In addition, granules were sampled from the full-scale Utrecht wastewater treatment plant during the

start-up phase, after seeding the reactor with Garmerwolde granules. Table 1 provides data regarding average influent characteristics for the treatment plants sampled. These granules will be collectively called 'full-scale' granules hereafter, unless otherwise noted.

Two types of granules were compared with the full-scale granules. Control beads were prepared by extracting structural EPS components from aerobic granules with acid and re-gelling them with $CaCl_2$ solution (Felz *et al.* 2016). The control EPS beads originate from AGS, but do not contain cells or the full suite of extracellular polymers present in full-scale granules. Second, saline laboratory granules, grown in synthetic wastewater with an added 5 g/L NaCl, were collected from a 3 L SBR at TU Delft (de Graaff *et al.* 2018). The saline granules contain microbes that would be expected to exist within the AGS samples from municipal wastewater reactors but were not exposed to complex substrates.

All samples, which ranged in volume from several hundred millilitres to several litres, were stored in airtight plastic containers in the refrigerator at 4 °C without substrate addition until the NMR measurements were performed. For the NMR imaging experiments, several granules (~5–10) were added to water in a 5 mm NMR sample tube. For the multidimensional correlation measurements, numerous granules (>> 10) were added to the 5 mm NMR sample tube without excess water to maximize the signal obtained from the granules relative to bulk water signal. Granules selected for NMR measurements were typically 2–4 mm in diameter to provide sufficient image pixels within the granule relative to the imaging field of view.

NMR measurements

^{1}H NMR is sensitive to hydrogen protons. In most biological systems, the dominant source of the NMR signal is water, although protons found in organic matter and extracellular polymers also contribute to the total signal. NMR image contrast depends on signal intensity and the signal relaxation rates of sample constituents (Van As & Lens 2001). Signal intensity is a function of the position **r** dependent proton density within a sample and applied magnetic field strength. The T_1 (or longitudinal) relaxation time and the T_2 (or transverse) relaxation time provide information on the physico-chemical environments in which different water populations exist (Callaghan 1991). T_1 relaxation is related to the timescale for the sample's net magnetization to return to thermal equilibrium following an excitation pulse. T_2 relaxation is related to molecular interactions that occur in the local magnetic field during the measurement. T_1 and T_2 relaxation occur on the order of seconds in bulk liquids and tens to hundreds of milliseconds in biofilms. Chemical exchange of protons between water and hydroxyl groups on polymer chains (Hills 1992) as well as the presence of rotationally restricted water in cells and the EPS matrix enhances T_2 relaxation in biofilms relative to bulk water. Controlling the timing of the radio-frequency (rf) pulses which make up magnetic resonance measurements can accentuate contrast between the various water populations without addition of chemical tracers. Further discussion of NMR theory is provided in Gjersing *et al.* (2005) and Callaghan (2011).

T_1 relaxation-weighted images show signal intensity at a single time, while $T_{2,\mathrm{eff}}$ maps, which are derived from a series of T_2 relaxation-weighted images, show rates of signal relaxation over a period of time. T_1 relaxation-weighted images will look different for the same granule depending on when the image was acquired during the measurement and are considered qualitative images. $T_{2,\mathrm{eff}}$ maps capture the entire signal decay quantitatively and are therefore more representative of the structure than any single T_1 relaxation-weighted image. T_1 relaxation- and T_2 relaxation-weighted ($T_{2,\mathrm{eff}}$) images were collected on an NMR spectrometer operating at 22.3 T (950 MHz) using

Table 1 | Average influent characteristics for sources of full-scale granules

Source	Population equivalent	COD (mg/L)	BOD_5 (mg/L)	TSS (mg/L)	TN/TKN (mg/L)	TP (mg/L)	Period	Reference
Garmerwolde, NL	140,000	506	224	236	49.4/-	6.7	2014	Pronk *et al.* (2015, 2017)
Vroomshoop, NL	12,000	720	263	317	-/66	9	2014	Pronk *et al.* (2017)
Utrecht, NL	430,000	660	247	300	58/-	8.2	Jun–Dec 2019	Unpublished data
Utrecht prototype, NL	9,000	732	289	385	74/-	13.4	2016	Unpublished data
Rockford demonstration, USA	300	142		111	19.4/-	1.8	Jun–Aug 2018	Unpublished data

COD: chemical oxygen demand; BOD_5: biochemical oxygen demand; TSS: total suspended solids; TN: total nitrogen; TKN: total Kjeldahl nitrogen; TP: total phosphorus.

an Avance III HD console, with a Micro5 imaging probe, maximum gradients 3 T/m, and a 5 mm birdcage coil (Bruker Biospin, Ettlingen, Germany) at the uNMR-nl national facility (Utrecht, The Netherlands) using parameters found in Table 2 for AGS samples from PNU and Garmerwolde, as well as the EPS and saline control granules. The matrix size was 128×128 and receiver bandwidth was 50 kHz. Note that parameters used for NMR images of Utrecht start-up granules, acquired at a later time on the 22.3 T system and shown in Figure 3, are different and are given in the caption to Figure 3. The NMR images of PNU granules were collected on both fresh granules (several days after sampling) and on aged samples (approximately 2 months after sampling). Granules from the Vroomshoop and Rockford treatment plants were not available at the time of image acquisition on the 22.3 T system. Measurement parameters for images of Vroomshoop, Garmerwolde, and Rockford AGS samples made on a Bruker Avance III system with a 5.9 T (250 MHz for protons) superconducting magnet are found in Table 3.

Multidimensional NMR experiments combine two pulse sequences such that the induced signal is encoded in multiple independent dimensions to explore how two parameters are related. In the T_1–T_2 relaxation correlation experiment, T_2 relaxation is measured for protons experiencing a given T_1 relaxation rate over a range of T_1 relaxation times. The measurement can be used to separate signal which overlaps in one domain or, as in this case, can provide insight into the mechanism behind enhanced signal relaxation. T_1–T_2 relaxation correlation experiments were performed on a 5.9 T superconducting magnet (250 MHz for protons) networked to a Bruker Avance III spectrometer and using a high rf power probe, a 5 mm rf coil, and a 5 mm sample tube. The correlation measurements were performed using an inversion recovery–CPMG sequence at 20 °C with a dwell time of 10 μs, an echo time, t_E, of 100 μs, 30,000 echoes, 32 inversion times between 1 ms and 50 s, and 16 averages.

Table 2 | NMR measurement parameters for multi-slice multi-echo images

	T_1-weighted	T_2-weighted	$T_{2,eff}$ map
Repetition time, T_r (ms)	550	5,000	5,000
Echo time, t_E (ms)	5.3	5.3	5.3
Number of echoes	16	16	32
X-Y resolution (μm)	47×47	47×47	47×47
Z-slice thickness (μm)	100	100	100
Number of averages	8	1	4
Duration	9 min 23 s	10 min 40 s	42 min

The 22.3 T NMR system at uNMR-NL, an NWO-funded National Roadmap Large-Scale Facility of the Netherlands, located at Utrecht University, produced high-resolution and high-contrast images with a minimal measurement time due to the field strength dependent signal intensity. Samples imaged at 22.3 T included AGS samples from PNU and Garmerwolde, as well as control EPS and saline granules. Parameters used for Utrecht granules imaged at 22.3 T are given in the Figure 3 caption.

Table 3 | NMR measurement parameters for multi-slice multi-echo images made at 5.9 T (250 MHz)

	$T_{2,eff}$ map
Repetition time, T_r (ms)	5,000
Echo time, t_E (ms)	5.6
Number of echoes	8
X-Y resolution (μm)	94×94
Z-slice thickness (μm)	500
Number of averages	32
Duration	2 h 50 min

The matrix size was 128×64 and the receiver bandwidth was 50 kHz. Samples imaged at 5.9 T included AGS samples from Vroomshoop and Rockford treatment plants, as well as control EPS beads.

Other microscopy

Aged granules from Garmerwolde were also imaged using transmission electron microscopy (TEM). Granules were fixed in 3% glutaraldehyde for 24 hours, cut into quarters, then returned to the glutaraldehyde solution. The granule quarters were subsequently treated according to Brumfield *et al.* (2009). Images were made using an LEO 912AB TEM (Zeiss) operated at 100 KV accelerating voltage and a $2{,}048 \times 2{,}048$ Proscan CCD camera.

Data analysis

$T_{2,eff}$ maps

Multi-slice multi-echo (MSME) imaging produces two-dimensional (2D) T_2 relaxation-weighted images showing the signal echo amplitude per voxel, or volume element, in each sample slice for a given t_E. An image is collected at times equal to n^*t_E, where n is the echo number, such that the stack of images for each slice shows the attenuation of signal in each voxel with time. Fitting the echo attenuation in each voxel as an exponential decay produces a 2D relaxation map of the sample where the pixel intensity corresponds to the effective relaxation rate, $R_{2,eff}$, or the effective relaxation time, $T_{2,eff}$. Since signal from protons experiencing restricted rotational mobility or chemical

exchange will experience enhanced relaxation, $T_{2,eff}$ maps are used to identify regions of varying cell and EPS densities (Edzes *et al.* 1998; Gonzalez-Gil *et al.* 2001; Gjersing *et al.* 2005). $T_{2,eff}$ relaxation times are significantly shorter than T_2 relaxation times measured without spatial resolution due, in part, to the influence of water diffusion across magnetic field gradients applied for imaging. Higher resolution images produce shorter $T_{2,eff}$ relaxation times. In addition, higher magnetic field strength and longer t_E also enhance relaxation (Edzes *et al.* 1998). Thus, $T_{2,eff}$ values are only comparable between images when the same magnetic field strength and measurement parameters are used across samples. $T_{2,eff}$ map data were analysed using Prospa ((v3.13) Magritek Ltd, Wellington, NZ).

T_1–T_2 relaxation correlation experiments

When data are collected from a sample exhibiting multi-exponential signal decay due to a range of relaxation domains, the data can be analysed by an inverse Laplace transform (ILT) in both dimensions. The 2D ILT was implemented in MATLAB (R2018a, MathWorks, Natick, MA, USA) using a non-negative least squares fitting function with a regularization parameter, α, to minimize the error in the solution (Hurlimann *et al.* 2002; Callaghan *et al.* 2003).

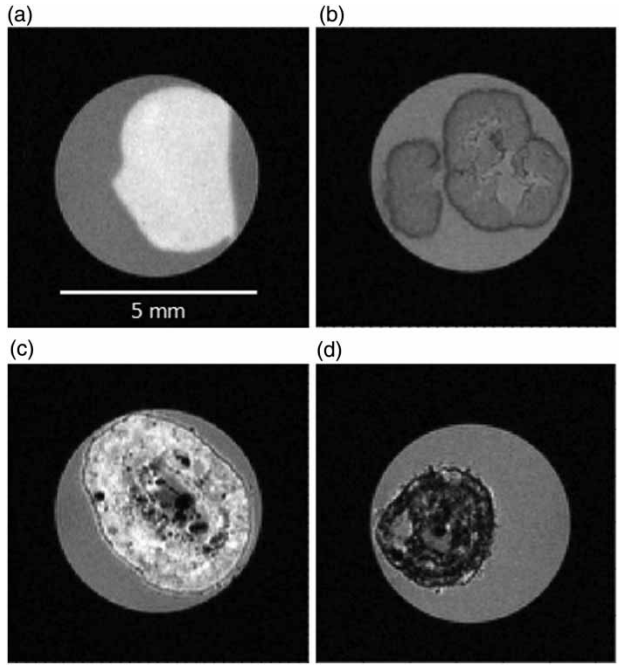

Figure 1 | T_1-weighted images. Compared to the control EPS bead (a) and saline laboratory granule (b), aerobic granules collected from the PNU reactor (c) and Garmerwolde treatment plant (d) show a heterogeneous internal structure. Lighter regions correspond to regions with diffuse EPS while darker areas suggest denser or highly cross-linked EPS and cell clusters. Black regions indicate a lack of signal due to either a solid inclusion, or signal relaxation on the timescale of the measurement, i.e. faster than 5.3 ms (950 MHz, 47 μm × 47 μm × 100 μm, $t_E = 5.3$ ms, $T_r = 550$ ms, 1st echo).

RESULTS AND DISCUSSION

The goal of this study was to identify internal structural features within aerobic granules from full-scale municipal wastewater treatment plants and determine how consistent those features are across granule sources and over time. T_1 and T_2 relaxation-weighted images of granules from wastewater treatment plants reveal heterogeneous internal structures where water molecules and biopolymers experience different degrees of rotational mobility and variable opportunities for chemical exchange as reflected in the T_1 and T_2 relaxation behavior. The NMR images presented here show an axial 'image slice' through a 5 mm NMR sample tube with water surrounding the intact granule. The NMR parameters, as defined in Table 2, are identical in all T_1-weighted images presented in Figure 1.

T_1 relaxation-weighted images

EPS beads (Figure 1(a)) and saline laboratory granules (Figure 1(b)) showed significantly different degrees of heterogeneity compared to the aerobic granules treating municipal wastewater (Figure 1(c) and 1(d)). The EPS beads were uniform and showed no discernible internal structure. This is attributable, in part, to the extraction method, which is selective for specific biopolymers. Saline granules showed a radial distribution of signal intensity with faster relaxation and more apparently dense regions on the outer surface and higher intensity, less dense regions in the center of the granules.

Images of granules from the PNU reactor and Garmerwolde treatment plant reflected spatially heterogeneous NMR signal intensity and relaxation behavior, though the AGS samples from PNU appeared to have a higher relative volume of brighter regions with slower T_2 relaxation than the Garmerwolde granules. It was significantly more difficult to collect high quality images from the Garmerwolde granules at 22.3 T due to their rapid signal decay at the ultra-high magnetic field, suggesting a denser structure overall in the EPS matrix or greater abundance of relaxation-enhancing components like paramagnetic ions (e.g. Fe(III)) and biopolymers with a high proportion of exchangeable protons. Granules from Vroomshoop and Rockford were not imaged at 22.3 T, though

imaging at lower magnetic field strength (5.9 T, see Figure 5) suggests that their internal structural properties are more similar to Garmerwolde granules than to PNU granules (Figure 2).

Figure 2 shows an assortment of fresh granules from the PNU reactor with characteristic dark, dense regions and brighter, less dense regions. Like Figure 1, these images are T_1-weighted with a short repetition time (T_r) of 550 ms to enhance signal from the gel-like regions of the granule with shorter T_1 times. They are also T_2-weighted since these images were collected with a t_E of 15.9 ms (third echo image) rather than the 5.3 ms (first echo image) shown in Figure 1. The granule pictured in the upper left corner is the same PNU granule shown in Figure 1(c). The combination of T_1- and T_2-weighting provides excellent contrast between regions with differing relaxation behavior. While these images show some variation between the individual granules with respect to size, shape, and spatial arrangement of more and less dense biopolymer and cell mass regions, the general form of internal structures (i.e. clusters) in the granules show similarity indicating consistency in NMR-visible properties among granules from the same reactor. Consistency in structural forms was also observed in granules imaged at 5.9 T. These structural similarities among granules from the same reactor (Figure 2), in conjunction with larger variation across different reactors (Figure 1), raise questions about the operational conditions under which these structures form and the range of function they support.

Research on NMR relaxation in the presence of proteins and polysaccharides shows that the bound water mechanism for T_2 relaxation enhancement is small compared to the influence of chemical exchange of protons between water molecules and functional groups in biopolymer solutions (Hills 1992). Macromolecules like proteins and polysaccharides provide more abundant exchangeable protons than cell membranes, making T_2 relaxation more sensitive to EPS density than to cell concentration (Beuling *et al.* 1998). Thus, lighter regions are interpreted as lower-density EPS regions while darker areas suggest more concentrated or more tightly cross-linked EPS, with the caveat that EPS components are complex and various constituents may provide more or fewer exchangeable proton sites. The EPS comprising the control bead has not been analysed to characterize the number of exchangeable protons but comparison of structures published for the extracted EPS (Lin *et al.* 2010) and Granulan (Seviour *et al.* 2012), another gel-forming component of structural EPS, suggests that there may be fewer exchangeable protons on the extracted EPS in the control bead than on other biopolymers known to exist in AGS. Moreover, since EPS is produced by active microbes, it can be surmised that the darker regions also indicate cell clusters. Lemaire and colleagues reported evidence suggesting that different bacterial populations

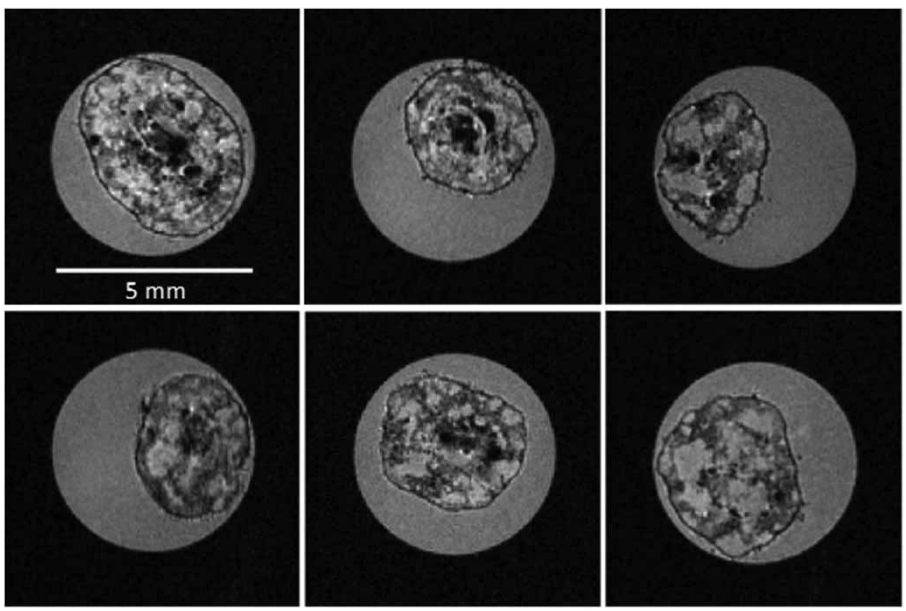

Figure 2 | Fresh granules from the Utrecht prototype SBR (PNU) with characteristic darker, dense EPS regions and brighter less dense EPS regions. Relatively bright bulk water is visible outside the granule in the 5 mm sample tube (950 MHz, 47 μm × 47 μm × 100 μm, $t_E = 15.9$ ms, $T_r = 550$ ms, 3rd echo).

produce different types of EPS and are associated with a range of cell densities (Lemaire *et al.* 2008). Black regions in the images indicate a lack of signal due to solid-like inclusions, gas bubbles, or signal relaxation, $T_{2,\text{eff}}$, on the timescale of the measurement (i.e. faster than 5.3 ms).

Images of granules from the new full-scale reactor at the Utrecht wastewater treatment facility sampled during the reactor start-up phase show what appears to be a core with fast T_2 relaxation typical of Garmerwolde structure overgrown by biomass (i.e. cells and EPS matrix) with relaxation characteristics and internal structures typical of PNU granules (Figure 3). Harvested Garmerwolde granules were used as seed sludge to inoculate the system at start-up while the influent wastewater comes from the same municipal source as the PNU reactor. Verawaty and co-workers observed that flocs labelled with fluorescent microbeads aggregated around crushed seed granules labelled with contrasting fluorescent microbeads in both batch and SBR systems. (Verawaty *et al.* 2012). After 80 days of SBR operation, Verawaty's experimental granules reflected a distribution where granule-labelled beads were located near the core and floc-labelled beads were located near the surface of the aggregates. Figure 3 appears to support the finding that seed granules can act as a template for new growth and suggests that the seed granules may retain their structural form while new biomass develops under the influence of current operating conditions. The NMR images of these granules therefore confirm that influent wastewater characteristics and reactor operations govern the formation of the internal structures observed within AGS. However, the controlling parameter(s) cannot be identified with these NMR images.

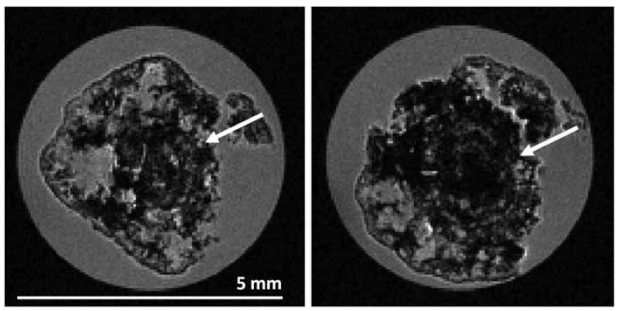

Figure 3 | T_1-weighted MSME images of two granules from the start-up phase of the full-scale Utrecht wastewater treatment plant. The faster relaxation in the center is characteristic of the seed granules from Garmerwolde wastewater treatment plant, while the outer shell (~700 μm) resembles the internal structure of a prototype Utrecht (PNU) granule. The white arrows indicate the apparent boundary between the old and the new growth. Bulk water visible outside the granule in the 5 mm sample tube provides a reference for the NMR parameter signal intensity weighting of free water (950 MHz, 35 μm × 35 μm × 100 μm, $t_E = 3.19$ ms, $T_r = 550$ ms, 2nd echo).

$T_{2,\text{eff}}$ maps

$T_{2,\text{eff}}$ maps of a control EPS bead and two granules from the PNU reactor are shown in Figure 4. One of the PNU granules was from a fresh, 4-day old sample (Figure 4(b)) while the other was 2 months old (Figure 4(c)), with both stored at 4 °C. Both PNU granules show the same heterogeneous internal structure observed in Figures 1 and 2. The $T_{2,\text{eff}}$ maps also show that neither the structure nor the $T_{2,\text{eff}}$ relaxation behavior changes significantly over the timescale of approximately 2 months. In both PNU $T_{2,\text{ eff}}$ maps, the bulk water $T_{2,\text{eff}}$ relaxation time is 18 ms, which is approximately equal to the maximum internal $T_{2,\text{eff}}$ time in the granule voids. In the dense regions of the granules, the minimum $T_{2,\text{eff}}$ times are approximately 6 ms with the apparent transition between voids and dense EPS occurring around a $T_{2,\text{eff}}$ time of 12 ms.

$T_{2,\text{eff}}$ maps of EPS beads collected with the same measurement parameters (Figure 4(a)) show low contrast between the effective relaxation times of bulk water and the EPS bead. The $T_{2,\text{eff}}$ maps produced the same bulk water relaxation time as the PNU maps, as expected, and a relatively uniform effective relaxation time within the bead of approximately 14.7 ms. This $T_{2,\text{eff}}$ is within the range of relaxation times found in the apparent voids in the PNU granules. The longer $T_{2,\text{eff}}$ relaxation times observed in the EPS beads, compared to the dense regions of the full-scale granules, may be due to the absence of other exopolymers that enhance relaxation. Because of the sensitivity to biopolymer structure with respect to exchangeable protons, time-domain NMR may be useful in identifying differences in EPS components that are not apparent in confocal micrographs of granules stained with fluorescein isothiocyanate for proteins, concanavalin A for α-polysaccharides, or calcofluor white for β-polysaccharides. Within the field of NMR spectroscopy, characterization of protein structure is well established (Banci *et al.* 2010), while characterization of polysaccharides remains a challenge. Thus, time-domain NMR imaging alone is not sufficient to identify and elucidate details of EPS content and structure but may be a useful guide to motivate further investigation with other methods, including NMR spectroscopy.

Several researchers (Stoodley *et al.* 1994; Wilking *et al.* 2013) have reported the possibility of liquid flow within a biofilm. Channels within the biofilm would permit convection and could potentially increase the penetration of a substrate into the biofilm. Ultra-high field NMR imaging with a spatial resolution of $19.5 \times 19.5 \times 100\ \mu m^3$ revealed the presence of fluid channels in extra-large (1,500–2,500 μm diameter) algal

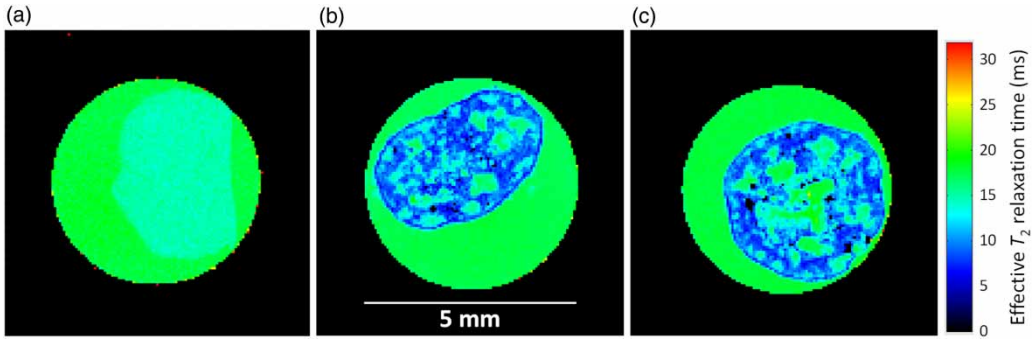

Figure 4 | $T_{2,eff}$ relaxation maps of a control EPS bead (a) and two granules from the PNU reactor. A 4-day old PNU granule (b) and a 2-month old PNU granule (c) show the same heterogeneous internal structure observed in Figures 1 and 2 and the same range of $T_{2,eff}$ values. The EPS bead (a) displays a homogeneous $T_{2,eff}$ time of approximately 14.7 ms which is within the range of that found in the voids of both PNU granules (b, c). The maps were produced from MSME images (32 echoes) made on the 22.3 T system in the national ultra-high field NMR laboratory in Utrecht, NL. Spatial resolution is $47 \times 47 \times 100$ microns.

colonies (Schadewijk *et al.* 2018). Observations of channels in aerobic granules have been made as well, albeit after extensive sample treatment (Ivanov *et al.* 2005; Lemaire *et al.* 2008; Gonzalez-Gil & Holliger 2014) in preparation for light microscopy and TEM. Both of these microscopy methods involve sectioning and dehydration of the granule or granule slice. It can therefore be questioned if the observed channels are an artefact of the sample preparation or if they are truly present in the intact granules. NMR imaging has potential to identify channel morphologies in intact and representative granules, since the method is non-invasive and non-destructive, provided the achievable spatial resolution is greater than the channel diameter.

The $T_{2,eff}$ relaxation maps of PNU granules in Figure 4(b) and 4(c)) reveal the presence of a large number of voids, distributed throughout the granule and a large cavity in the center of the aged granule (Figure 4(c)). The similarity of $T_{2,eff}$ times in Figure 4(a) (bulk liquid and EPS) and granule voids in Figure 4(b) and 4(c) suggests that the voids are in fact filled with water and a small fraction of EPS or EPS with few exchangeable proton sites. In these images, the voids do not appear to be connected to the outside bulk liquid but instead are separated by biomass (cells and EPS) with distinctively different relaxation behavior. It should be noted that the spatial resolution of NMR images presented here ($47 \times 47 \times 100$ μm) is relatively low compared to traditional microscopy and is lower than that applied in the algal colonies where channels were observed (Schadewijk *et al.* 2018). A channel with a diameter smaller than the spatial resolution will be hard to detect with NMR, though ultra-high field magnetic resonance has potential to further improve resolution limits. The channels reported by Gonzalez-Gil & Holliger (2014) are estimated to be roughly 50 μm in diameter, approximately the detection limit in this study. These NMR results suggest that channels with a diameter larger than 50 μm and connected to the bulk fluid are not present in aerobic granules imaged here and that convection may play a limited role in substrate transport in the granule interior.

$T_{2,eff}$ maps of granules from Vroomshoop and Rockford were made using the 5.9 T (250 MHz) system. Figure 5 shows a representative longitudinal slice through a stack of granules in water in the 5 mm NMR sample tube and highlights the variability observed both within and across granule sources. These granules again show heterogeneous internal structure and appear to be more similar to Garmerwolde granules than to granules from the PNU reactor. In the Rockford granules there appears to be more of a concentric ring structure than is apparent in PNU granules, and the less dense EPS regions appear to be less numerous but larger in volume. There are few locations in both samples with relaxation times equal to the bulk water value. The Vroomshoop granules exhibit more of a cluster structure than concentric rings and most closely resemble Garmerwolde granules of all the granules imaged in this study. Despite the internal structural differences between the granule sources, a similar range of relaxation times is apparent in Vroomshoop and Rockford granules, ranging from less than 10 ms in the dense biomass to more than 40 ms in the less dense EPS regions. The bulk water relaxation in both cases is approximately 50 ms. Since the magnetic field strength, imaging gradient strengths, and spatial resolution are different between Figures 4 and 5, the values of $T_{2,eff}$ are not directly comparable. The lower spatial resolution and lower magnetic field strength on the 5.9 T system produce a wider range of $T_{2,eff}$ times within the biofilm, while the ultra-high field 22.3 T system provides high contrast and resolution of chemical exchange between

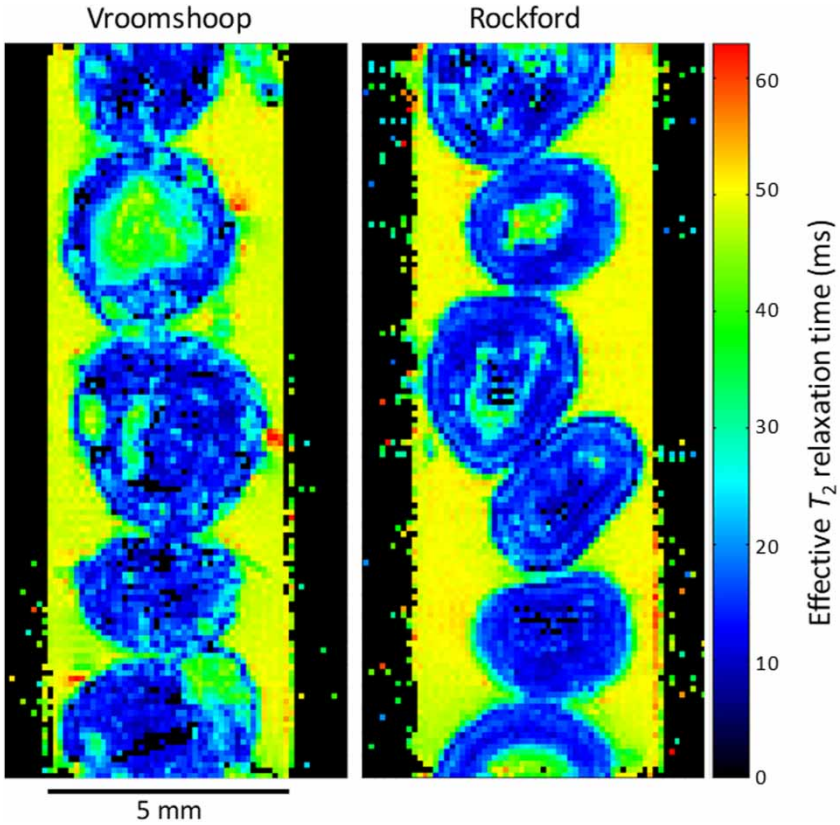

Figure 5 | $T_{2,eff}$ maps of granules from the Vroomshoop (left) and Rockford (right) treatment plants show a longitudinal slice through a stack of granules in water in the 5 mm NMR sample tube. The two samples contain a similar range of relaxation times and provide an example of the variability of relaxation times within granules from the same reactor and between treatment plants. The maps were produced from MSME images (8 echoes) made on the 5.9 T system. Spatial resolution is $94 \times 94 \times 500$ microns.

biopolymer species in the NMR imaging experiments shown in Figures 1–3.

T_1–T_2 relaxation correlations

In addition to imaging experiments, 2D T_1–T_2 relaxation correlation measurements were collected. These measurements confirm the presence of multiple T_2 populations and a distribution of T_1 populations within the granules. Since these data were collected without spatial resolution, the resulting distributions reflect the range and relative proportion of relaxation times inherent in the sample and are not subject to enhanced relaxation related to imaging.

T_1–T_2 relaxation correlations were measured for 1-month-old Vroomshoop granules without bulk water using the 250 MHz (5.9 T) system (Figure 6). The measurements were made using intact granules (left) and the same sample after crushing the granules in the sample tube (right). The broad T_1–T_2 correlation for the intact granules reflects the presence of spatial heterogeneities that exist across length scales many orders of magnitude larger than the length scale of molecular interactions between water and biopolymers. The distribution approaches the T_1–T_2 parity line at longer relaxation times, indicating highly mobile water populations in the voids, and diverges from the parity line at shorter relaxation times. The short relaxation times indicate water in the pores of a highly cross-linked EPS matrix where the biopolymer signal may exhibit more solid-like behavior. Because of the spatial heterogeneity of the internal structural features, even highly mobile water in a void would not experience the dense EPS of a cluster over the timescale of the measurement, resulting in the broad T_1–T_2 correlation observed. After crushing the granules, the T_1–T_2 correlation shows the loss of the population with larger T_1 and T_2 relaxation times, corresponding to the very diffuse EPS regions in the granules where molecular interactions are limited on the timescale of the measurement. Homogenization of the biofilm minimizes the length scale of heterogeneity, allowing interactions between hydrogen-bearing species previously

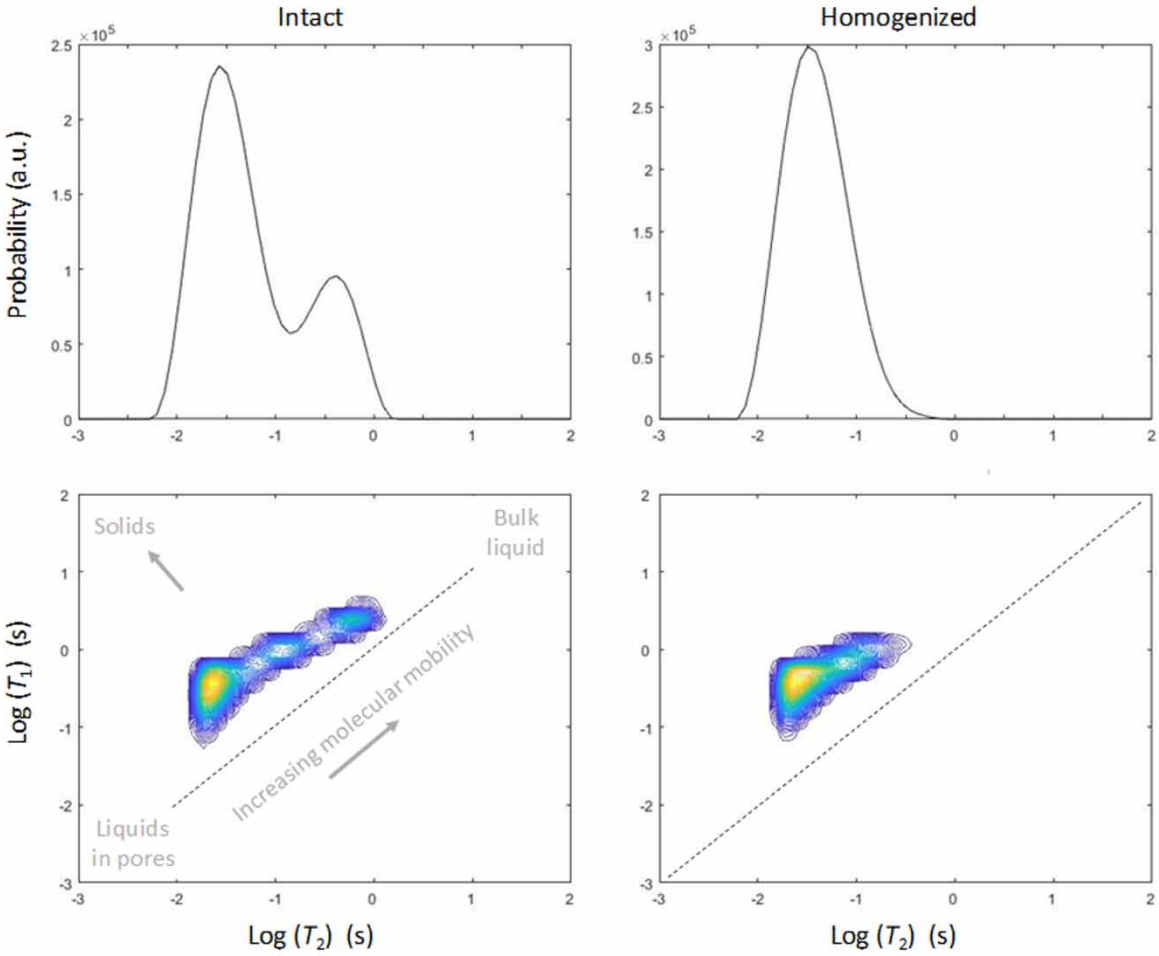

Figure 6 | The T_1–T_2 correlation measured on the 5.9 T system on a stack of 1-month-old Vroomshoop granules (left), and the same sample after homogenization inside the NMR sample tube (right). The loss of the population with the longer T_1 and T_2 times, corresponding to water populations in the granule voids, confirms that the internal granule structures are responsible for the distribution of relaxation times observed.

separated in space. Water molecules previously in the void regions can undergo chemical exchange of protons with EPS after homogenization, leading to a decrease in the maximum T_2 relaxation time. Physically breaking the structure of the granules may also have entangled polymers that were spatially separated, increasing the rotational correlation time of the biopolymers previously in the voids. This would also lead to a decrease in the maximum T_1 relaxation time, as was observed. These measurements provide further confirmation that the structure of the granule is responsible for the distribution of relaxation times observed in the NMR measurements. Thus, the observed relaxation times in the NMR images are a clear indicator of different local physical and chemical environments and point to the importance of chemical exchange of protons in the relaxation response.

Apparent 'boundary layer'

An apparent 'boundary layer' was observed as a thin dark layer on the surface of the municipal AGS samples imaged at 22.3 T but was not observed on the EPS beads. The layer was approximately 1 pixel wide (~50 μm) in the NMR data. The darkness of the layer in the image could be attributed to a lack of signal (fewer protons), or very fast signal relaxation. To eliminate the possibility that the 'boundary layer' was simply an artefact of the measurement at the ultra-high magnetic field, a granule from PNU was cut in half with a razor blade and imaged in the 22.3 T system (Figure 7(a)). The layer is visible on the undisturbed outer surface of the granule but not on the cut edge, suggesting that the physico-chemical properties of the surface are indeed different from the center of the granule. An NMR

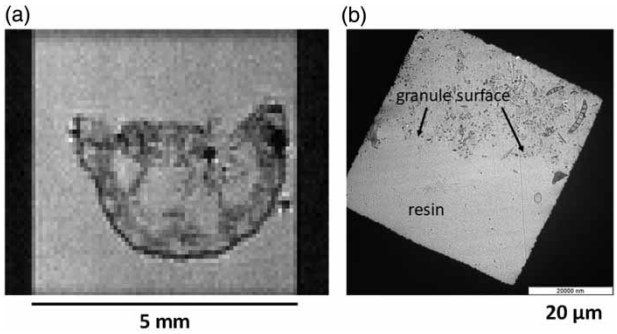

Figure 7 | A PNU granule cut in half and imaged at 22.3 T (950 MHz) (a) shows the dark apparent 'boundary layer' on the outer surface of the granule, but no such layer on the cut edge, suggesting that the layer is not an artefact of the measurement. A TEM image of the outer surface of an aged Garmerwolde granule (b) shows a dense cell layer but not inorganic material that might explain the 'boundary layer'.

artefact would be expected to be visible on the cut edge as well.

As part of the effort to identify the cause of the apparent boundary layer observed with NMR, images were also made using TEM to more directly observe the surface layer of aerobic granules from the Garmerwolde treatment plant. Inorganic debris and solid particulates that might be present in municipal wastewater would be visible under TEM. Figure 7(b) shows dense cell clusters at the surface of a granule in the top of the image, with the embedding resin outside of the granule at the bottom. There was no precipitate or solid particulate debris visible on any granule surface examined with TEM. Research is ongoing to determine the source of the apparent boundary layer and to determine if the same mechanism is responsible for the apparent ring structure that can be seen in the $T_{2,\mathrm{eff}}$ relaxation maps of Rockford granules shown in Figure 5 or in the Garmerwolde granule in Figure 1.

CONCLUSIONS

Even though the structure of aerobic granular sludge is directly linked to mass transport and conversion processes in the granules, our understanding of the granule structure and the mechanisms by which it forms is still quite limited. In this paper, state-of-the-art ultra-high field and non-invasive magnetic resonance methods were used to explore the structural characteristics of full-scale and laboratory-scale granules. NMR provides the ability to screen larger samples sizes of intact granules and can, therefore, help to provoke and answer questions related to structure and function, as well as the reliability and representativeness of data collected via more labor intensive and destructive microscopy methods. NMR results indicated that aerobic granules from municipal treatment plants exhibit a heterogeneous structure comprised of variable density EPS and cell clusters, and water-like voids. The structures observed were either similar to the cluster structure observed in some anaerobic granules (Gonzalez-Gil *et al.* 2001) or similar to a concentric ring structure with each granule source having a characteristic type. The structures in all granules were stable over a storage period of several months. The NMR data further revealed an apparent boundary layer, which appeared to be of organic origin and cannot be attributed to measurement artefact or accumulation of inorganic material on the granule surface. The granules did not contain channels larger than 50 μm, but rather apparent voids containing water and diffuse EPS or exopolymers with few exchangeable protons. These observations highlight the complex structure of aerobic granules and the need for non-invasive characterization methods such as NMR that can provide unique data on the granule structure.

ACKNOWLEDGEMENTS

This material is based upon work supported by the National Science Foundation (NSF) Graduate Research Fellowship Program under Grant No. DGE-1049562. Further support comes from the Graduate Research Opportunities Worldwide Program which is jointly funded by NSF and the Netherlands Organisation for Scientific Research (NWO), as well as from a VIDI grant funded by NWO (no. 016.168.320). J.R.K. was supported by the NWO-funded Netherlands' Magnetic Resonance Research School (NMARRS) graduate school (022.005.029). Any opinions, findings, and conclusions or recommendations expressed in this material are those of the author(s) and do not necessarily reflect the views of NSF or NWO. Experiments at the 22.3 T (950 MHz) NMR instrument were supported by uNMR-NL, an NWO-funded National Roadmap Large-Scale Facility of the Netherlands (project 184.032.207). The authors also thank Susan Brumfield at Montana State University for the TEM imaging and the late Paul T. Callaghan for providing the ILT software.

DATA AVAILABILITY STATEMENT

All relevant data are included in the paper or its Supplementary Information.

REFERENCES

Banci, L., Bertini, I., Luchinat, C. & Mori, M. 2010 NMR in structural proteomics and beyond. *Progress in Nuclear Magnetic Resonance Spectroscopy* **56** (3), 247–266. https://doi.org/10.1016/j.pnmrs.2009.12.003.

Beuling, E. E., van Dusschoten, D., Lens, P., van den Heuvel, J. C., Van As, H. & Ottengraf, S. P. P. 1998 Characterization of the diffusive properties of biofilms using pulsed field gradient-nuclear magnetic resonance. *Biotechnology and Bioengineering* **60** (3), 283–291. https://doi.org/10.1002/(sici)1097-0290(19981105)60:3 < 283::aid-bit3 > 3.3.co;2-q.

Beun, J. J., van Loosdrecht, M. C. M. & Heijnen, J. J. 2002 Aerobic granulation in a sequencing batch airlift reactor. *Water Research* **36** (3), 702–712. https://doi.org/10.1016/s0043-1354(01)00250-0.

Brumfield, S. K., Ortmann, A. C., Ruigrok, V., Suci, P., Douglas, T. & Young, M. J. 2009 Particle assembly and ultrastructural features associated with replication of the lytic archaeal virus *Sulfolobus* turreted icosahedral virus. *Journal of Virology* **83** (12), 5964–5970. https://doi.org/10.1128/jvi.02668-08.

Callaghan, P. 1991 *Principles of Nuclear Magnetic Resonance Microscopy*. Oxford University Press, Oxford, UK.

Callaghan, P. T. 2011 *Translational Dynamics and Magnetic Resonance: Principles of Pulsed Gradient Spin Echo NMR*. Oxford University Press, Oxford, UK.

Callaghan, P. T., Godefroy, S. & Ryland, B. N. 2003 Diffusion-relaxation correlation in simple pore structures. *Journal of Magnetic Resonance* **162** (2), 320–327. https://doi.org/10.1016/s1090-7807(03)00056-9.

Chen, M.-Y., Lee, D.-J., Tay, J.-H. & Show, K.-Y. 2007 Staining of extracellular polymeric substances and cells in bioaggregates. *Applied Microbiology and Biotechnology* **75** (2), 467–474. https://doi.org/10.1007/s00253-006-0816-5.

Codd, S. L., Seymour, J. D., Gjersing, E. L., Gage, J. P. & Brown, J. R. 2006 Magnetic resonance microscopy of biofilm and bioreactor transport. In: *NMR Imaging in Chemical Engineering* (S. Stapf & S.-I. Han, eds). Wiley, USA.

de Bruin, L. M. M., de Kreuk, M. K., van der Roest, H. F. R., Uijterlinde, C. & van Loosdrecht, M. C. M. 2004 Aerobic granular sludge technology: an alternative to activated sludge? *Water Science and Technology* **49** (11–12), 1–7.

de Graaff, D. R., van Dijk, E. J. H., van Loosdrecht, M. C. M. & Pronk, M. 2018 Strength characterization of full-scale aerobic granular sludge. *Environmental Technology* **41**, 1637–1647. https://doi.org/10.1080/09593330.2018.1543357.

de Kreuk, M. K. & van Loosdrecht, M. C. M. 2006 Formation of aerobic granules with domestic sewage. *Journal of Environmental Engineering-ASCE* **132** (6), 694–697. https://doi.org/10.1061/(asce)0733-9372(2006)132:6(694).

Edzes, H. T., van Dusschoten, D. & Van As, H. 1998 Quantitative t-2 imaging of plant tissues by means of multi-echo MRI microscopy. *Magnetic Resonance Imaging* **16** (2), 185–196. https://doi.org/10.1016/s0730-725x(97)00274-9.

Felz, S., Al-Zuhairy, S., Aarstad, O. A., van Loosdrecht, M. C. M. & Lin, Y. M. 2016 Extraction of structural extracellular polymeric substances from aerobic granular sludge. *JoVE-Journal of Visualized Experiments* **115**. https://doi.org/10.3791/54534

Gjersing, E. L., Codd, S. L., Seymour, J. D. & Stewart, P. S. 2005 Magnetic resonance microscopy analysis of advective transport in a biofilm reactor. *Biotechnology and Bioengineering* **89** (7), 822–834. https://doi.org/10.1002/bit.20400.

Gonzalez-Gil, G. & Holliger, C. 2014 Aerobic granules: microbial landscape and architecture, stages, and practical implications. *Applied and Environmental Microbiology* **80** (11), 3433–3441. https://doi.org/10.1128/aem.00250-14.

Gonzalez-Gil, G., Lens, P. N. L., Van Aelst, A., Van As, H., Versprille, A. I. & Lettinga, G. 2001 Cluster structure of anaerobic aggregates of an expanded granular sludge bed reactor. *Applied and Environmental Microbiology* **67** (8), 3683–3692. https://doi.org/10.1128/aem.67.8.3683-3692.2001.

Hills, B. P. 1992 The proton exchange cross-relaxation model of water relaxation in biopolymer systems. *Molecular Physics* **76** (3), 489–508. https://doi.org/10.1080/00268979200101491.

Hurlimann, M. D., Venkataramanan, L. & Flaum, C. 2002 The diffusion-spin relaxation time distribution function as an experimental probe to characterize fluid mixtures in porous media. *Journal of Chemical Physics* **117** (22), 10223–10232.

Ivanov, V., Tay, S. T. L., Liu, Q. S., Wang, X. H., Wang, Z. W. & Tay, J. H. 2005 Formation and structure of granulated microbial aggregates used in aerobic wastewater treatment. *Water Science and Technology* **52** (7), 13–19.

Kagawa, Y., Tahata, J., Kishida, N., Matsumoto, S., Picioreanu, C., van Loosdrecht, M. C. M. & Tsuneda, S. 2015 Modeling the nutrient removal process in aerobic granular sludge system by coupling the reactor- and granule-scale models. *Biotechnology and Bioengineering* **112** (1), 53–64. https://doi.org/10.1002/bit.25331.

Lemaire, R., Webb, R. I. & Yuan, Z. G. 2008 Micro-scale observations of the structure of aerobic microbial granules used for the treatment of nutrient-rich industrial wastewater. *ISME Journal* **2** (5), 528–541. https://doi.org/10.1038/ismej.2008.12.

Lens, P. N. L., Gastesi, R., Vergeldt, F., van Aelst, A. C., Pisabarro, A. G. & Van As, H. 2003 Diffusional properties of methanogenic granular sludge: ^{1}H NMR characterization. *Applied and Environmental Microbiology* **69** (11), 6644–6649. https://doi.org/10.1128/aem.69.11.6644-6649.2003.

Lin, Y., de Kreuk, M., van Loosdrecht, M. C. M. & Adin, A. 2010 Characterization of alginate-like exopolysaccharides isolated from aerobic granular sludge in pilot-plant. *Water Research* **44** (11), 3355–3364. https://doi.org/10.1016/j.watres.2010.03.019.

Liu, L., Sheng, G.-P., Liu, Z.-F., Li, W.-W., Zeng, R. J., Lee, D.-J., Liu, J.-X. & Yu, H.-Q. 2010 Characterization of multiporous structure and oxygen transfer inside aerobic granules with the percolation model. *Environmental Science & Technology* **44** (22), 8535–8540. https://doi.org/10.1021/es102437a.

McSwain, B. S., Irvine, R. L., Hausner, M. & Wilderer, P. A. 2005 Composition and distribution of extracellular polymeric substances in aerobic flocs and granular sludge. *Applied and*

Environmental Microbiology **71** (2), 1051–1057. https://doi.org/10.1128/aem.71.2.1051-1057.2005.

Pronk, M., de Kreuk, M. K., de Bruin, B., Kamminga, P., Kleerebezem, R. & van Loosdrecht, M. C. M. 2015 Full scale performance of the aerobic granular sludge process for sewage treatment. *Water Research* **84**, 207–217. https://doi.org/10.1016/j.watres.2015.07.011.

Pronk, M., Giesen, A., Thompson, A., Robertson, S. & van Loosdrecht, M. 2017 Aerobic granular biomass technology: advancements in design, applications and further developments. *Water Practice and Technology* **12** (4), 987–996. https://doi.org/10.2166/wpt.2017.101.

Schadewijk, R. v., Berg, T. E. v. d., Gupta, K. B. S. S., Ronen, I., de Groot, H. J. M. & Alia, A. 2018 Non-invasive magnetic resonance imaging of oils in *Botryococcus braunii* green algae: chemical shift selective and diffusion-weighted imaging. *PLoS ONE* **13** (8), e0203217. https://doi.org/10.1371/journal.pone.0203217.

Seviour, T., Yuan, Z., van Loosdrecht, M. C. M. & Lin, Y. 2012 Aerobic sludge granulation: a tale of two polysaccharides? *Water Research* **46** (15), 4803–4813. https://doi.org/10.1016/j.watres.2012.06.018.

Stoodley, P., Debeer, D. & Lewandowski, Z. 1994 Liquid flow in biofilm systems. *Applied and Environmental Microbiology* **60** (8), 2711–2716.

Tay, J. H., Liu, Q. S. & Liu, Y. 2001 The role of cellular polysaccharides in the formation and stability of aerobic granules. *Letters in Applied Microbiology* **33** (3), 222–226. https://doi.org/10.1046/j.1472-765x.2001.00986.x.

Van As, H. & Lens, P. 2001 Use of ^{1}H NMR to study transport processes in porous biosystems. *Journal of Industrial Microbiology & Biotechnology* **26** (1–2), 43–52.

Verawaty, M., Pijuan, M., Yuan, Z. & Bond, P. L. 2012 Determining the mechanisms for aerobic granulation from mixed seed of floccular and crushed granules in activated sludge wastewater treatment. *Water Research* **46** (3), 761–771. https://doi.org/10.1016/j.watres.2011.11.054.

Weissbrodt, D. G., Neu, T. R., Kuhlicke, U., Rappaz, Y. & Holliger, C. 2015 Assessment of bacterial and structural dynamics in aerobic granular biofilms (Reprinted from *Frontiers in Microbiology* **4**, 175, 2013). In: *Bioremediation of Wastewater: Factors and Treatment* (O. Sanchez, ed.). Apple Academic Press, Oakville, ON, Canada, 141–174.

Wilen, B.-M., Liebana, R., Persson, F., Modin, O. & Hermansson, M. 2018 The mechanisms of granulation of activated sludge in wastewater treatment, its optimization, and impact on effluent quality. *Applied Microbiology and Biotechnology* **102** (12), 5005–5020. https://doi.org/10.1007/s00253-018-8990-9.

Wilking, J. N., Zaburdaev, V., De Volder, M., Losick, R., Brenner, M. P. & Weitz, D. A. 2013 Liquid transport facilitated by channels in *Bacillus subtilis* biofilms. *Proceedings of the National Academy of Sciences* **110** (3), 848. https://doi.org/10.1073/pnas.1216376110.

Xavier, J. B., De Kreuk, M. K., Picioreanu, C. & Van Loosdrecht, M. C. M. 2007 Multi-scale individual-based model of microbial and bioconversion dynamics in aerobic granular sludge. *Environmental Science & Technology* **41** (18), 6410–6417. https://doi.org/10.1021/es070264 m.

First received 28 February 2020; accepted in revised form 13 July 2020. Available online 27 July 2020